Journal of Materials Chemistry A

ROYAL SOCIETY OF CHEMISTRY

PAPER

View Article Online
View Journal

Cite this: DOI: 10.1039/d5ta09854h

On the transport properties of $K_2ZnV_2O_7$

Esther M. Curtis,[a] Kehan Kuang,[b] Josie E. Auckett,[ca] Stephen J. Skinner[bd] and Ivana Radosavljević Evans[*a]

$K_2ZnV_2O_7$ has recently been reported as a promising oxide ion conductor. We have studied this material using a number of structure- and physical property-probing techniques. Our extensive characterisation using variable temperature synchrotron X-ray and neutron diffraction, impedance spectroscopy and tracer diffusion measurements of its transport properties, does not support the reports that $K_2ZnV_2O_7$ undergoes partial reduction at high temperatures, leading to the creation of vacancies and oxide ion conductivity. In particular, the lack of oxide ion diffusion observed by isotope exchange definitively rules out oxide ion conductivity within $K_2ZnV_2O_7$. Instead, we find that the high conductivity measured originates from the melting of a small amount of KVO_3 impurity in the sample, which is detectable by synchrotron X-ray and neutron diffraction.

Received 2nd December 2025
Accepted 23rd December 2025

DOI: 10.1039/d5ta09854h

rsc.li/materials-a

Introduction

High oxide ion conductivity was recently reported in $K_2ZnV_2O_7$, describing its performance ($\sigma = 1.14 \times 10^{-3}$ S cm^{-1} at 600 °C) as similar to that of yttria-stabilised zirconia (YSZ) which is used as an electrolyte in solid oxide fuel cells (SOFCs).[1] The high oxide ion conductivity was ascribed to the formation of intrinsic vacancies caused by the reduction of some V^{5+} to V^{4+} at temperatures above 400 °C, and the formula of the highly conducting material was given as $K_2ZnV_2O_{6.64}$. Despite the significant proportion of mixed valent vanadium ($K_2ZnV^{5+}{}_{1.28}V^{4+}{}_{0.72}O_{6.64}$) that corresponds to the proposed composition at high temperatures, a two-probe Hebb-Wagner polarisation measurement was used to rule out electronic conductivity contribution. A further four-probe Hebb-Wagner measurement was used to rule out K^+ ion conduction. On this basis, $K_2ZnV_2O_7$ was described as a promising pure oxide ion conductor and has since gained interest as a potential SOFC electrolyte material.[1,2]

Our interest in $K_2ZnV_2O_7$ stemmed from its anisotropic structure and the possibility of investigating its oxide ion conductivity by measurements on large oriented single crystals,[3–9] with a view of property optimisation in device-ready forms. Here we report the preparation and characterisation of polycrystalline $K_2ZnV_2O_7$ which we undertook as the initial step in the originally intended single crystal growth. Our extensive characterisation by several techniques, including variable temperature synchrotron X-ray and neutron diffraction, impedance spectroscopy and oxygen isotope tracer diffusion measurements of its transport properties, does not support the claim that $K_2ZnV_2O_7$ is an oxide ion conductor.

Experimental

Synthesis

Polycrystalline sample of $K_2ZnV_2O_7$ was synthesised using traditional solid-state synthesis. Stoichiometric amounts of K_2CO_3 (≥99.0%, Sigma-Aldrich), ZnO (99.9%, Sigma-Aldrich) and NH_4VO_3 (99+%, Sigma-Aldrich), were weighed out, ground and sintered at 350 °C for 15 h. The powder was ground, pressed into pellets and fired at 600 °C for 12 h. This was repeated until the sample was pure by laboratory powder X-ray diffraction (PXRD).

Structural characterisation

For structural characterisation and assessment of phase purity, we have performed variable temperature laboratory X-ray, synchrotron X-ray and neutron diffraction experiments. All diffraction data were analysed using the Rietveld method[10] implemented in the TOPAS Academic software.[11,12]

Laboratory powder X-ray diffraction. PXRD patterns were collected on a Bruker D8 Advance diffractometer with a Lynx-Eye PSD detector and monochromatic Cu Kα radiation (λ = 1.5406 Å). The patterns used to monitor the progress of the solid-state reaction were collected at room temperature in the 2θ range 10–90° with a data collection time of 20–30 minutes. The pattern of the final polycrystalline sample was collected in the 2θ range 10°–120° with a data collection time of 10 hours.

[a]Department of Chemistry, Durham University, Lower Mountjoy, South Road, Durham, DH1 3LE, UK. E-mail: ivana.radosavljevic@durham.ac.uk
[b]Department of Materials, Imperial College London, Exhibition Road, London, SW7 2AZ, UK
[c]Australian Synchrotron, ANSTO, 800 Blackburn Road, Clayton VIC 3168, Australia
[d]International Institute for Carbon Neutral Energy Research, Kyushu University, Fukuoka, Japan

Variable temperature synchrotron powder X-ray diffraction. Variable temperature synchrotron PXRD data were collected on the Powder Diffraction beamline at the Australian Synchrotron.[13] The sample was loaded into a 0.3 mm diameter capillary which was rotated during data collection. Patterns were collected on heating and cooling between 30 and 500 °C in 10 °C steps, using a ramp rate of 10 °C min and 30 s equilibration time at each temperature. Refined parameters included unit–cell parameters, atomic positions, isotropic atomic displacement parameters, sample height, a background polynomial and pseudo-Voigt peak shape function terms.

Variable temperature powder neutron diffraction. High intensity time-of-flight (TOF) neutron powder diffraction patterns were collected on the Polaris instrument at the ISIS Neutron and Muon source, Rutherford Appleton Laboratory.[14] A sample of $K_2ZnV_2O_7$ weighing 3.62 g was packed into an 8 mm cylindrical vanadium can, giving a sample height of 47 mm. Data collections were performed for 8 h at room temperature and 550 °C using the RAL furnace. Additional 30-minute data sets were collected at 20 °C intervals between 30 °C and 550 °C. Simultaneous Rietveld refinement of the $K_2ZnV_2O_7$ structural model[1] against all 5 detector banks on the Polaris instrument was carried out. In the final cycles, the main phase $K_2ZnV_2O_7$ was modelled with freely refining atomic fractional coordinates and anisotropic atomic displacement parameters (ADPs). As vanadium has a very low neutron scattering length (Coh b = 0.3824 fm), the vanadium fractional coordinates were constrained to the atomic position obtained from our room temperature synchrotron $K_2ZnV_2O_7$ data; for the same reason, the ADP of the vanadium was constrained to the Zn isotropic ADP. The fractional occupancy of each O site was refined freely. The impurity phase, KVO_3, was modelled using the same peak shape as the main phase. The atomic coordinates were freely refined, with the exception of vanadium, which was restrained to the literature value.[15] Isotropic ADPs were refined for each atom type, with the vanadium isotropic ADP constrained to the potassium ADP.

Physical property characterisation

AC impedance spectroscopy. AC impedance spectroscopy data were collected on a 10 mm diameter pellet sintered at 600 °C for 12 h, with a relative density of 84%, coated with Au paste (Metalor Technologies) for use as electrodes. The sample was mounted on a Probostat A-6 cell and the electrodes were fired at 600 °C for 30 min. Impedance measurements were collected in air in approximately 20 °C intervals between 300–600 °C with a ramp rate of 2 °C min^{-1} and a frequency range of 0.1 – 10^7 Hz. Data were analysed by simple circuit fitting using the ZView/Zplot software (Scribner Associates).

Differential scanning calorimetry. Differential scanning calorimetry (DSC) was collected in air by a PerkinElmer 8500, using CP grade helium, with a flow rate of 20 ml min^{-1}, as a purge gas. Standard aluminium pans were used and the sample was heated and cooled between room temperature and 600 °C with a ramp rate of 10 °C min^{-1}.

Tracer diffusion measurements. Oxygen isotope tracer diffusion measurements were collected on a 10 mm diameter pellet sintered at 600 °C for 12 h. The pellet was halved and one half was coated with Ag paste, while the other half was left uncoated. Both halves were fired at 550 °C for 30 min. The pellets were placed in a quartz chamber under a vacuum of < 5.0 × 10^{-8} mbar. The samples were pre-annealed (513 °C, 8 h, 200 mbar of $^{16}O_2$) and quenched. The chamber was evacuated to < 5.0 × 10^{-8} mbar and the sample isotopically exchanged at 514 °C for 2 h under 200 mbar of $^{18}O_2$ ($[^{18}O_2]/[^{16}O_2+^{18}O_2] \approx 81\%$).

To collect long-range tracer diffusion data, the line scan method was used.[16] The tracer diffusion measurements were conducted using a TOF-SIMS 5 instrument (ION-TOF GmbH, Germany). The measurements were performed under high vacuum conditions (<1 × 10^{-8} mbar). The primary ion gun was a Bi^{3+} liquid metal ion gun (LMIG), and an electron flood gun was used during the measurements for charge compensation. The measurement area was set to 300 × 300 μm. The collected data were analysed using SurfaceLab 7 software (ION-TOF GmbH, Germany).

Results and discussion

Fig. S1a and S1b show the Rietveld fits obtained using the laboratory and synchrotron PXRD data collected on the same sample. Both data sets confirm that the structure of $K_2ZnV_2O_7$ is melilite-related, with the *c*-axis doubled relative to the melilite archetype due to the ordering of K^+ ions on two crystallographically unique sites. While the sample appears to be phase-pure by laboratory PXRD (Fig. S1a), extra peaks are observed in the synchrotron PXRD pattern. They could be assigned to KVO_3, which was included as the second phase in the Rietveld fitting of the synchrotron data, giving an excellent fit (Fig. S1b). The KVO_3 content at room temperature refined to 4.4(1) wt%.

Sequential Rietveld fitting of the variable temperature synchrotron PXRD data show that the KVO_3 peaks (marked with arrows in Fig. 1) disappear between 470 °C and 490 °C on heating and reappear between 460 °C and 420 °C on cooling. Since the melting point of pure KVO_3 is 530 °C,[17] we attribute this change to the melting and recrystallisation of the small amount of this phase present in the $K_2ZnV_2O_7$ sample.

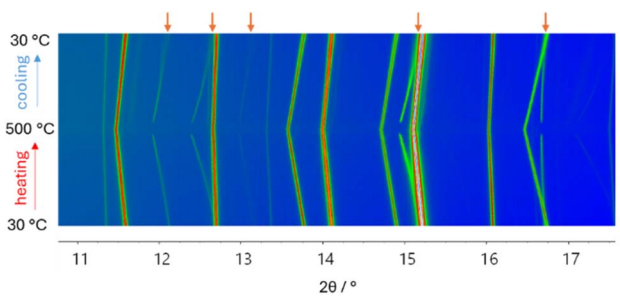

Fig. 1 Surface plot of the synchrotron PXRD patterns collected between 30 – 500 °C. Peaks belonging to the KVO_3 impurity, shown with orange arrows, disappear between 470 °C and 490 °C on heating and reappear between 460 °C and 420 °C on cooling.

The DSC measurement (Fig. 2a) on the same sample shows an endothermic peak on heating and an exothermic counterpart on cooling, with a hysteresis of about 40 °C (exo- and endothermic peaks at 519 °C and 483 °C, respectively), consistent with melting and recrystallisation.

A similar abrupt change is observed in the data obtained by impedance spectroscopy (Fig. 2b). The total conductivity changes reversibly by four orders of magnitude between 440 and 530 °C (from 3.9 (9) × 10^{-7} S cm^{-1} to 1.14 (2) × 10^{-3} S cm^{-1}); this change is accompanied by a hysteresis of about 40 °C, comparable to that observed for the disappearance and reappearance of the KVO_3 peaks in the diffraction data. We therefore attribute this increase in conductivity to the melting of a small amount of the KVO_3 impurity present in the sample, and the significant contribution of the molten phase to the total conductivity measured. Wei *et al.*[1] also reported a jump in conductivity, but they attributed it to the reduction of some V^{5+} to V^{4+} and formation of vacancies leading to oxide ion conductivity. The magnitude of the reported conductivity change (from ~2 × 10^{-7} S cm^{-1} at 350 °C to ~4 × 10^{-5} S cm^{-1} at 400 °C) is smaller and it occurs at a slightly lower temperature compared to our observations, which is presumably related to different quantities of the KVO_3 present in different samples.

While Wei *et al.* describe their sample as pure, a small number of weak features not predicted for $K_2ZnV_2O_7$ can be seen in their room-temperature powder neutron diffraction pattern (Fig. 8b in ref. 1), most notably at a *d*-spacing of 2.43 Å, corresponding to the (041) reflection of KVO_3. This reflection is also present in our neutron diffraction data and is marked with an arrow in Fig. S2a. Two-phase Rietveld fit to our room-temperature neutron diffraction data gave an excellent agreement between the observed and calculated patterns, with the KVO_3 impurity content refined to 2.91(6) wt%.

The oxygen atom content per formula unit as a function of temperature, obtained from our variable-temperature neutron diffraction data fitting, is shown in Fig. 3. This analysis shows that in the temperature range investigated the composition does not deviate from $K_2ZnV_2O_7$, in contrast to the previous report which gave a composition $K_2ZnV_2O_{6.64}$ above 400 °C.[1] In addition, the unit cell parameters extracted from our Rietveld analysis of neutron diffraction data show a smooth variation of

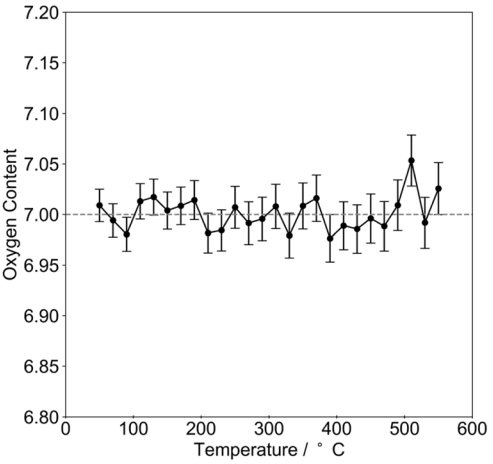

Fig. 3 Oxygen atom content per formula unit of $K_2ZnV_2O_7$ as function of temperature obtained from variable-temperature neutron diffraction data. The grey dashed line indicated the fully stoichiometric oxygen content.

temperature (Fig. S3), consistent with the absence of any phase transitions or even subtle structural changes in the unit cell parameters which would likely reflect the reduction of 36% of V^{5+} into V^{4+}, given the difference in the atomic radii of the two species (0.35 Å and ~0.50 Å, respectively).[18] Anisotropic atomic displacement parameters (ADPs) from structure refinements against neutron diffraction data are given in Fig. S4.

Oxide ion diffusion in $K_2ZnV_2O_7$ can be directly probed using $^{18}O_2$ isotopic exchange followed by secondary ion mass spectrometry (SIMS) measurements. When exposed to an $^{18}O_2$-enriched atmosphere, ^{18}O exchanges at the sample surface and subsequently diffuses inward, producing a concentration depth profile. This profile follows Fick's laws of diffusion for a semi-infinite medium, enabling quantitative analysis by SIMS to determine the diffusion coefficient.

Wei *et al.*[1] report that the oxide ion conductivity is comparable to that in YSZ, and therefore, the exchange conditions were designed similarly to those used for YSZ, assuming oxide ion diffusivity of ~7 × 10^{-9} cm^2 s^{-1} at 500 °C.[19] From this the exchange time and depth required for the $K_2ZnV_2O_7$ sample were estimated. The surface exchange coefficient of oxygen in $K_2ZnV_2O_7$ is expected to be low and an Ag coating was used to enhance this.[1] The resulting diffusion profile of $K_2ZnV_2O_7$ was expected to be similar to that of YSZ using these exchange parameters.

Fig. 4a and b show the normalised isotopic ratio of the oxide ion ([$^{18}O^-$]/[$^{16}O^-$+$^{18}O^-$]) diffusion profile of both uncoated and Ag-coated samples after being isotopically exchanged with $^{18}O_2$ at 514 °C, respectively. No clear diffusion profile is observed for either sample, suggesting that there is only very limited oxide ion diffusion, if any. The concentration of the oxygen isotope as a function of depth is only fractionally above the level expected from the natural abundance of ^{18}O in the sample. The large signal fluctuation is due to the low $^{18}O^-$ counts. The normalised isotopic ratio in the Ag-coated sample is slightly higher than that of the uncoated one. Additionally, an $^{18}O^-$ signal drop in

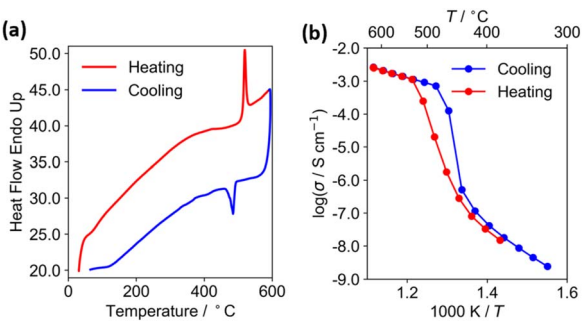

Fig. 2 (a) DSC traces between room temperature and 600 °C. (b) Arrhenius plot of the total conductivity between 300 °C and 600 °C on heating and cooling.

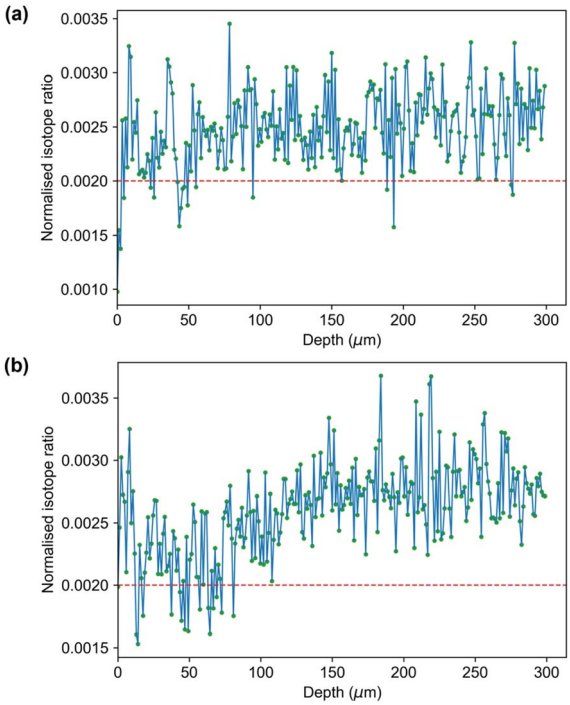

Fig. 4 Normalised oxide ion ($[^{18}O^-]/[^{16}O^-+^{18}O^-]$) diffusion profile of (a) bare and (b) Ag-coated samples, respectively. The red dashed lines indicate the $^{18}O^-$ natural abundance.

the Ag-coated sample was found at a depth of around 50 μm. From the secondary ion image (Fig. S5b), an amorphous layer was formed in a similar region, suggesting Ag could potentially react with $K_2ZnV_2O_7$, which might modify the morphology and alter the $^{18}O^-$ counts. This amorphous layer was not observed in the uncoated sample (Fig. S5a). As both samples do not exhibit an oxygen diffusion profile and show a low concentration for ^{18}O species it is evident that this composition does not possess any oxide ion transport. This definitively rules out oxide ion conductivity in $K_2ZnV_2O_7$ and further supports the reinterpretation of the high conductivity as due to the presence of molten KVO_3 above 530 °C.

Conclusions

We have studied $K_2ZnV_2O_7$ using a number of structure- and physical property-probing techniques to investigate the recent claim of high oxide ion conductivity in this material. Our extensive characterisation using variable temperature synchrotron X-ray and neutron diffraction, impedance spectroscopy and tracer diffusion measurements of its transport properties, does not support the previous report that $K_2ZnV_2O_7$ undergoes partial reduction at high temperatures, leading to the creation of vacancies and oxide ion conductivity. Instead, we find that the high conductivity measured originates from the melting of a small amount of KVO_3 impurity in the sample, which is detectable by synchrotron X-ray and neutron diffraction.

Conflicts of interest

There are no conflicts to declare.

Data availability

Data supporting this article are available in the supplementary information (SI) document. Supplementary information: additional structural and property characterisation data. See DOI: https://doi.org/10.1039/d5ta09854h.

Acknowledgements

The authors thank the Leverhulme Trust for the provision of a PhD research project grant for EMC (RPG-2023-080). SJS thanks the RAEng for the award of a Research Chair (RCSRF/1243-2021) and the authors acknowledge the support of the European Union's Horizon 2020 research and innovation program under grant agreement No. 101017709 (EPISTORE). IRE thanks Durham University for research leave. We thank Douglas Carswell (Durham University) for the assistance with DSC measurements, Dr Qinfen Gu (Australian Synchrotron) and Dr Paul Henry (ISIS Neutron and Muon Source) for the assistance with synchrotron PXRD and PND data collections.

Notes and references

1 H. Wei, J. Hao, J. Yang, Y. Lv, F. Shen, W. Zhang, J. Chen, L. He, L. Liu, X. Kuang and J. Xu, *ACS Mater. Au*, 2023, **3**, 492–500.
2 J. Li, Y. Liu, D. Liu, E. Y. Yang, Y. Zhang, X. Shi and C. Li, *Materials Science and Engineering: B*, 2026, **323**, 118692.
3 S. Nakayama and M. Highchi, *J. Mater. Sci. Lett.*, 2001, **20**, 913–915.
4 S. Nakayama, M. Sakamoto, M. Higuchi, K. Kodaira, M. Sato, S. Kakita, T. Suzuki and K. Itoh, *J. Eur. Ceram. Soc.*, 1999, **19**, 507–510.
5 M. Higuchi, K. Kodaira and S. Nakayama, *J. Cryst. Growth*, 2000, **216**, 317–321.
6 S. Nakayama and M. Sakamoto, *Solid State Ionics*, 2013, **253**, 47–52.
7 T. An, T. Baikie, F. Wei, S. S. Pramana, M. K. Schreyer, R. O. Piltz, J. F. Shin, J. Wei, P. R. Slater and T. J. White, *Chem. Mater.*, 2013, **25**, 1109–1120.
8 Y. Masubuchi, M. Higuchi, S. Kikkawa, K. Kodaira and S. Nakayama, *Solid State Ionics*, 2004, **175**, 357–360.
9 E. M. Curtis, J. E. Auckett and I. R. Evans, *CrystEngComm*, 2025, **27**, 7834–7841.
10 H. M. Rietveld, *J. Appl. Crystallogr.*, 1969, **2**, 65.
11 R. E. Dinnebier, A. Leineweber and J. S. O. Evans, *Rietveld Refinement: Practical Powder Diffraction Pattern Analysis Using TOPAS*, De Gruyter, 2010.
12 A. A. Coelho, J. Evans, I. Evans, A. Kern and S. Parsons, *Powder Diffr.*, 2011, **26**, S22.
13 K. S. Wallwork, B. J. Kennedy and D. Wang, *AIP Conf. Proc.*, 2007, **879**, 879–882.

14 R. I. Smith, S. Hull, M. G. Tucker, H. Y. Playford, D. J. McPhail, S. P. Waller and S. T. Norberg, *Rev. Sci. Instrum.*, 2019, **90**, 115101.
15 F. C. Hawthorne and C. Calvo, *J. Solid State Chem.*, 1977, **22**, 157–170.
16 J. A. Kilner, S. J. Skinner and H. H. Brongersma, *J. Solid State Electrochem.*, 2011, **15**, 861–876.
17 V. Volkov and A. Ivakin, *Zh. Neorg. Khim.*, 1986, **31**, 452–488.
18 R. D. Shannon and C. T. Prewitt, *Acta Cryst. B*, 1969, **25**, 925–946.
19 P. S. Manning, J. D. Sirman, R. A. De Souza and J. A. Kilner, *Solid State Ionics*, 1997, **100**, 1–10.